



Synthesis of Fe₃O₄/Bi₂WO₆ nanohybrid for the photocatalytic degradation of pharmaceutical ibuprofen under solar light



Tahereh Rohani Bastami^a, Ali Ahmadpour^{b,*}, Fatemeh Ahmadi Hekmatikar^b

^a Department of Chemical Engineering, Quchan University of Advanced Technology, Quchan, P.O. Box 94771-67335, Islamic Republic of Iran

^b Department of Chemical Engineering, Ferdowsi University of Mashhad, Mashhad, Islamic Republic of Iran

ARTICLE INFO

Article history:

Received 22 December 2015

Received in revised form 29 September 2016

Accepted 2 March 2017

Available online 10 March 2017

Keywords:

Magnetic properties

Photocatalysis

Fe₃O₄/Bi₂WO₆

Degradation

Solar light

ABSTRACT

Magnetic Fe₃O₄/Bi₂WO₆ nanohybrids were prepared via a two-step approach. Fe₃O₄ nanospheres were synthesized using a solvothermal method in polyol media and Bi₂WO₆ nanocrystals were formed by the subsequent hydrothermal process. In the preparation process of Bi₂WO₆ nanoparticles, tungstophosphoric acid hydrate (H₃PW₁₂O₄₀) was used as an acidic agent. The activity of the photocatalyst was evaluated by the photocatalytic degradation of ibuprofen (IBP) from an aqueous solution with solar light. The as-prepared nanohybrid, which could be easily recovered by a magnet, showed high efficiency in photocatalytic degradation of IBP, especially at pH = 4.7.

© 2017 The Korean Society of Industrial and Engineering Chemistry. Published by Elsevier B.V. All rights reserved.

Introduction

Ibuprofen (IBP), 2-[4-(2-methylpropyl) phenyl] propanoic acid belongs to the category of non-steroidal anti-inflammatory drugs which are widely used for the treatment of musculature pain, inflammatory disorders, fever, migraine, and tooth aches [1]. It has been reported that several kilotons of IBP are produced annually in the world, part of which being rejected to the effluents and excreted by patients [2,3]. The reported concentration of IBP in the environment is in the range of 10 ng L⁻¹–169 μg L⁻¹ [4]. IBP is not biodegradable in the municipal wastewater treatment plants. Thus, several techniques have been proposed for the removal or degradation of this pollutant [5,6]. These degradation techniques include advanced oxidation processes such as gamma irradiation [2], pulse radiolysis [7], ultrasonic irradiation [8], solar photo-Fenton [9], photocatalysis and sonophotocatalysis [10,11]. Among these methods, photocatalysts is often adopted for the degradation of organic pollutant like pharmaceutical compounds from aqueous media. Catalytic processes are both efficient and low cost [12–16]. Semiconductor photocatalysts have gained attention due to their wide application in photocatalytic degradation of organic compounds. In this context, a semiconductor based on Aurivillius oxides seems to be suitable for photocatalytic application [12].

Bismuth tungstate (Bi₂WO₆), a member of the Aurivillius oxide family with the general formula of Bi₂A_{n-1}B_nO_{3n+3} (A = Ca, Sr, Ba, Pb, Bi, Na, K and B = Ti, Nb, Ta, Mo, W, Fe) is an ideal candidate for the visible-light-driven photocatalytic material [17,18]. However, it is not easy to reuse and recycle photocatalysts due to the difficulty of its recovery from aqueous media. In fact, the reusability of photocatalysts is a major concern of industrial applications [12]. The use of magnetic-photocatalyst nanomaterials can be promising as they both allow easy recovery by an external magnetic field and demonstrate high degradation efficiency [19].

To facilitate the separation of catalysts and photocatalysts, researchers have immobilized the photocatalytic active materials onto iron oxides [20,21]. These immobilized materials lead to convenient and economic separation via an external magnetic field. It has been shown that the immobilization of photocatalysts onto magnetic nanoparticles can accelerate the efficient separation of catalyst from aqueous media [22]. There are many reports on the synthesis of photocatalyst nanocomposites using Fe₃O₄ nanoparticles [22,23] with some focusing on the preparation of magnetic photocatalyst by means of bismuth compounds [12,24]. Since Bi₂WO₆ and Fe₃O₄ have different crystalline structures, the Bi₂WO₆ cannot be directly grown on the surface of iron oxide. To overcome this problem, Chen et al. coated SiO₂ with Fe₃O₄ to improve bonding [12]. Zhang et al. used carbon to coat the surface of iron oxide, which provided a reactive interlayer for the production of Bi₂WO₆@carbon/Fe₃O₄ core-shell structure [22].

In this study, a simple synthesis approach was adopted to prepare magnetite nanosphere with hydrophilic surface in polyol

* Corresponding author.

E-mail addresses: t.rohani@qjet.ac.ir (T. Rohani Bastami), ahmadpour@um.ac.ir, ahmadpour_ir@yahoo.com (A. Ahmadpour).

media. The synthesis of Fe_3O_4 nanoparticles in the ethylene glycol as polyol media provided active sites for the adsorption of WO_4^{2-} , which was favorable for connecting Bi_2WO_6 to magnetite nanoparticles. Thus, the bismuth tungstate was connected to the surface active sites of Fe_3O_4 nanoparticles. To the best of our knowledge, there are no reports regarding the degradation of IBP by $\text{Fe}_3\text{O}_4/\text{Bi}_2\text{WO}_6$ photocatalysts under the solar light. In addition, to introduce tungstophosphoric acid hydrate ($\text{H}_3\text{PW}_{12}\text{O}_{40}$) as the Keggin type of polyoxometalates (POM) into the structure of Bi_2WO_6 , it was used as an acidic agent in the preparation of bismuth tungstate. Recently, there have been growing studies on the green synthesis of metal nanoparticles using POMs as photocatalysts, mild reductants and stabilizers [25–29]. The purpose of the present work is to investigate the photocatalytic activity of this magnetic nano hybrid for solar degradation of IBP as a model of nonsteroidal anti-inflammatory drug (NSAID) in water. The impact of reaction conditions such as contact time, solution pH, photo-Fenton catalytic activity and different additives were also checked. Fe^{2+} ions from the Fe_3O_4 core were also involved in the Fenton process, which could improve the efficiency of IBP decomposition.

Materials and methods

Materials

All chemicals were of analytical grade and used without further purification. Iron (III) chloride hexahydrate ($\text{FeCl}_3 \cdot 6\text{H}_2\text{O}$), sodium acetate anhydrous (NaAC), ethylene glycol anhydrous, sodium tungstate dehydrate ($\text{Na}_2\text{WO}_4 \cdot 2\text{H}_2\text{O}$), tungstophosphoric acid hydrate ($\text{H}_3\text{PW}_{12}\text{O}_{40}$) (Keggin type of POM), hydrogen peroxide (30%), isopropanol, and sodium hydrogen carbonate (NaHCO_3) were purchased from Merck Company. Bismuth nitrate pentahydrate ($\text{Bi}(\text{NO}_3)_3 \cdot 5\text{H}_2\text{O}$) and Ibuprofen (IBP), $\text{C}_{13}\text{H}_{18}\text{O}_2$, were purchased from Sigma-Aldrich Company and Shandong Xinhua Pharmaceutical Company in China. Milli-Q water was used with a minimum resistivity of $18.2 \text{ M}\Omega \text{ cm}^{-1}$.

Preparation of magnetite (Fe_3O_4) nanosphere

Magnetite nanospheres were synthesized by the modified solvothermal method in a polyol medium, as described elsewhere [30,31]. In brief, $\text{FeCl}_3 \cdot 6\text{H}_2\text{O}$ (1.35 g) was dissolved in 40 mL of ethylene glycol to make a clear solution. Sodium acetate (3.6 g) was added to the above solution during stirring. The as-prepared slurry was sealed by Teflon-lined autoclave and maintained at 180°C for 12 h. After cooling to room temperature, the black precipitates (Fe_3O_4) were recovered magnetically and dried at the room temperature. According to the recent studies [30,31], the above-discussed reaction conditions were selected to obtain uniform shape and size of Fe_3O_4 nanoparticles.

Preparation of $\text{Fe}_3\text{O}_4/\text{Bi}_2\text{WO}_6$ nano hybrids

$\text{Bi}(\text{NO}_3)_3 \cdot 5\text{H}_2\text{O}$ (0.97 g, 2 mmol) and Fe_3O_4 (0.2 g) (the optimum ratio of Bi: Fe_3O_4 was obtained experimentally) were mixed in 5 mL of $\text{H}_3\text{PW}_{12}\text{O}_{40}$ (0.84 mM) at room temperature, and the mixture was sonicated for 30 min. After aging for 2 h, 30 mL of $\text{Na}_2\text{WO}_4 \cdot 2\text{H}_2\text{O}$ (1 mmol) solution was added. Then, the mixture was sonicated at room temperature for 30 min before being transferred to a Teflon-lined autoclave and maintained at 160°C for 24 h. After being cooled to the autoclave to room temperature, the orange product was separated magnetically, washed several times and finally dried at 50°C overnight.

Characterization

The composition and crystal phase of samples were characterized by X-ray diffraction (XRD) on a X'Pert Pro MPD X-ray diffractometer equipped with Cu irradiation ($\lambda = 1.5406 \text{ \AA}$). The size and morphology of samples were characterized by transmission electron microscopy (TEM) (CM 120 Philips, Netherlands). The sample was dispersed in ethanol and dropped on the copper grid before loading to the instrument. The FTIR of samples were recorded by Thermo Nicolet Avatar 370 FTIR in the range of $400\text{--}4000 \text{ cm}^{-1}$. The magnetization curve of synthesized magnetic-photocatalyst nano hybrid was investigated using VSM (Vibrating sample magnetometer, Leckeshore model). The optical properties of the magnetic-photocatalyst nano hybrid were determined by a UV-vis spectroscopy (Analytik Jena, Spekol 1300). To clarify intermediate products, the HPLC analysis was performed by the HPLC system of KNAUER consisting of solvent delivery pump (k-1001), and UV-vis detector (k-2600). Separation was performed at C18 column ($250 \times 4.6 \text{ mm}$; $5 \mu\text{m}$). The mobile phase used in this study was H_2O :acetonitrile (80:20, v/v) at 1.0 mL min^{-1} flow rate with detection at 220 nm. The mobile phase was filtered and degassed daily before usage [32].

Greater details of the chemical structure were investigated using X-ray photoelectron

spectroscopy (XPS) survey, which was carried out using a TWEEN ANODE XR3E2 X-ray photoelectron spectrophotometer with X-ray source.

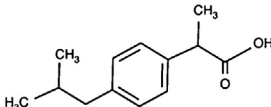
Point of zero charge measurement

The pH_{pzc} of the $\text{Bi}_2\text{WO}_6/\text{Fe}_3\text{O}_4$ nano hybrids was measured by the salt addition method [30].

Photocatalytic activity test

Photocatalytic activities of $\text{Fe}_3\text{O}_4/\text{Bi}_2\text{WO}_6$ nano hybrids were evaluated by degrading ibuprofen (chemical structure is shown in Table 1) under solar light irradiation as compared to dark condition. In each experiment, 70 mg of $\text{Fe}_3\text{O}_4/\text{Bi}_2\text{WO}_6$ nano hybrids was dispersed and stirred into 50 mL of IBP solution

Table 1
Chemical properties of IBP.

Pharmaceutical name	Chemical structure	MW (g mol^{-1})	pKa
Ibuprofen		206.29	4.9

(10 mg L⁻¹) and then illuminated under solar light (clear sky) with constant stirring at a temperature of 27–32 °C (GPS coordinates: N = 36°18'41.6", E = 59°31'54.2"). Some other experiments were run under dark condition for comparison. The experiments under solar light and dark conditions were run in a beaker of 600 mL. The thickness of nanophotocatalyst suspension was about 8 mm.

After each run, the samples were separated by an external magnetic field and centrifuged at 12,000 rpm for 10 min to complete the separation of photocatalyst from aqueous solution. The concentration of IBP solutions were analyzed using Spekol 1300 UV-vis. spectrophotometer at $\lambda = 224$ nm. In the case of pH study, the initial pH was adjusted by HCl and NaOH solutions and then measured by a pH-meter (HANNA instruments, Inc.).

Photocatalytic reactor

The optical thickness is a dimensionless parameter that signifies the number of scattering and absorption that may occur when light travels through the entire depth of the reactor, and shown in [33,34]:

$$\tau = (\sigma + \kappa)\delta C_{cat} \quad (1)$$

where τ (dimensionless) is optical thickness, σ (mL mg⁻¹, cm⁻¹) is specific mass scattering coefficient, κ is specific mass absorption coefficient, δ (cm) is reactor thickness, C_{cat} (mg ml⁻¹) is catalyst concentration and $\varepsilon = (\sigma + \kappa)$ is the extinction coefficient of the catalyst.

To determine extinction coefficient (ε , mL mg⁻¹, cm⁻¹) for nanophotocatalyst, the UV-vis spectroscopy was used over the range of 200–900 nm in three different concentrations (mg mL⁻¹) by dissolving a known mass of dry solid in a known volume of milli-Q water. The extinction coefficient of each case was determined by plotting the absorbance ($\lambda = 500$ nm) against concentration and subsequent linear regression analysis based on Beer-Lambert law ($Abs = \varepsilon \cdot c \cdot l$). [35]. All spectra showed a broad absorption between 400 and 600 nm centered at approximately 500 nm. The optical thickness (τ (Eq. (1)) estimated in our photoreactor for a Fe₃O₄/Bi₂WO₆ nanophotocatalyst loading of 1.4 mg mL⁻¹ and a depth of liquid of 8 mm was equal to 5.51.

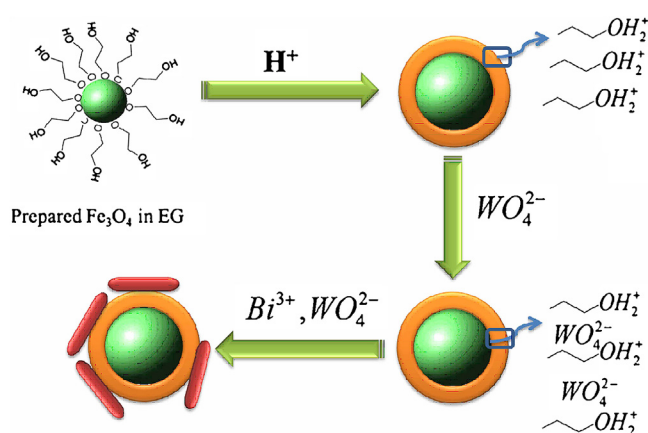
The optical thickness of photoreactor is a function of the extinction coefficient ($\sigma + \kappa$), thickness of the reaction space δ and the concentration of photocatalyst C_{cat} . The optical thickness takes the physical meaning of the ratio of reaction space thickness divided by photons mean free path in the suspension. In fact, the optical thickness is a measure of photoreactor's opacity with great optical thickness causing poor irradiation [36].

Results and discussion

Preparation and characterization of Fe₃O₄/Bi₂WO₆ nanohybrids

Bi₂WO₆ is one of the simplest Aurivillius oxides with a layered structure and a provskite-like slab WO₆, while the face-centered cubic Fe₃O₄ belongs to the inverse spinel structure [22]. In general, the Bi₂WO₆ nanostructure is unable to directly grow on the surface of Fe₃O₄ nanoparticles as a result of different crystalline structures.

As illustrated in Scheme 1, the synthesis strategy of Fe₃O₄/Bi₂WO₆ is carried out in the following stages. The Fe₃O₄ nanospheres are synthesized by the solvothermal method in polyol media. The synthesis of Fe₃O₄ nanoparticles in ethylene glycol (EG) generates the hydrophilic surface of the Fe₃O₄ nanospheres with a distribution of OH groups on their surfaces. After rapid protonation of magnetite nanoparticles surface, Bi₂WO₆ nanocrystals are formed by the subsequent hydrothermal process. According to Scheme 1, some of Bi₂WO₆ nanocrystals are



Scheme 1. The synthetic strategy for Fe₃O₄/Bi₂WO₆ preparation.

connected to the active sites on the surface of magnetite nanoparticles.

The X-ray diffraction patterns of Fe₃O₄/Bi₂WO₆ sample are shown in Fig. S1. The XRD peaks can be identified with tetragonal Bi₂WO₆ as the russellite phase (ICDD-00-026-1044, space group I41/amd, $a = b = 5.48$ Å, $c = 11.50$ Å) and the face-center cubic Fe₃O₄ phase (ICDD-98-001-2126, space group Fd-3m, $a = b = c = 8.34$ Å).

Some diffraction peaks of Fe₃O₄/Bi₂WO₆ assigned to Bi₂WO₆ at 2θ values of 28.3°, 32.9°, 36.3°, 47.3°, 56.2°, 58.8°, 68.7°, 76.3°, and 78.5° correspond to the crystal planes of (103), (200), (220), (303), (202), (107), (400), (109), and (307), respectively. Some of peaks assigned to the Fe₃O₄ at 2θ values of 18°, 30.8°, 35.1°, 37.2°, 43.3°, 53.9°, 57.4°, and 62.8° correspond to (111), (022), (113), (222), (004), (224), (115), and (044) respectively. No other phases of possible impurity were detected. In Fig. S1, there is a background in the XRD pattern which is due to poor crystallinity and small average grain-size of the products with large number of broken bonds at the surface. This confirms the nanosized and distorted surface morphology [37]. The average crystallite size of Bi₂WO₆ products along the (103) plane is calculated from the Scherrer equation (8 nm).

$$D = \frac{k\lambda}{\beta \cos \theta} \quad (2)$$

where λ is the wavelength of the X-ray radiation, k is the Scherrer constant ($k = 0.9$), θ is the characteristic X-ray radiation and β is the full-width at half maximum (FWHM) of the peaks.

Figs. S2 and S3 show the FTIR spectra of Fe₃O₄, as prepared by Bi₂WO₆, and Fe₃O₄/Bi₂WO₆ before and after the photocatalytic treatment. According to results, the peaks near 575 cm⁻¹ are attributed to Fe-O-Fe vibration of magnetite phase [12]. The peak appeared around 567 cm⁻¹ (red shift) after photocatalytic treatment (Fig. S3d). It is assumed that this minor red shift is due to weak interaction of ibuprofen molecules onto the surface of nanophotocatalyst. Figs. S2b and S3b show the FTIR spectrum as prepared by Bi₂WO₆. Peaks at 738 cm⁻¹ and 580 cm⁻¹ are assigned to the stretching vibration modes of Bi-O and W-O, respectively [38]. The 1384 cm⁻¹ and 1630 cm⁻¹ peaks are caused by C-H and O-H deformation vibration modes of adsorbed H₂O molecule [39]. In Figs. S2c and S2d, the broad absorption peaks of the samples observed around 3340 cm⁻¹ could be assigned to ν OH vibration of loosely-bonded (physisorbed) water molecules. The absorption bands of Bi₂WO₆ at 400–1700 cm⁻¹ were attributed to Bi-O-Bi, W-O stretching and W-O-W bridging stretching modes respectively [40]. Also, the W-O and W-O-W stretching bands could be attributed to the absorption bands of tungstophosphoric acid hydrate, interacting with Fe₃O₄/Bi₂WO₆ nanostructure

[41]. After the photocatalytic treatment of the sample, the FTIR results confirmed that small amount of organic molecules were adsorbed onto the surface of magnetic nano-hybrids so that most IBP molecules could be removed from the surface under solar light condition.

Fig. 1 shows the TEM image of the product. As can be seen, the Fe_3O_4 nanospheres with an average diameter of 84 nm were prepared and some needle-like Bi_2WO_6 nanoparticles were connected to the surface of magnetite nanoparticles. As shown in Fig. 1a and b, there are some bare magnetite nanoparticles in the prepared samples. Nitric acid has been shown to be a key factor in the formation of Bi_2WO_6 with a nano-architecture regular shape [42]. Also, studies reveal that three-dimensional (3D) irregular hierarchical umbilicate microsphere could be formed in the absence of nitric acid. Gui et al. investigated the influence of

pH on the morphology of hydrothermal products of Bi_2WO_6 [43]. They showed that irregular individual platelets with a smooth surface prevailed by increasing pH to 9.0, which also increased the edge size to 0.3–1 μm [43]. In this study, tungstophosphoric acid hydrate ($\text{H}_3\text{PW}_{12}\text{O}_{40}$) (Keggin type) was used instead of nitric acid and the needle-like nanostructures with numerous nanoparticles of irregular shapes and sizes, which were dispersed randomly on them, were obtained. Fig. 1c shows the size distribution of Fe_3O_4 nanoparticles, which confirms the uniform size and shape of synthesized magnetite nanoparticles.

The plot of magnetization versus magnetic field (M–H loop) at room temperature for $\text{Fe}_3\text{O}_4/\text{Bi}_2\text{WO}_6$ is illustrated in Fig. 2. A saturation magnetization (M_s) value of 15 emu/g was obtained, which is significantly less than the corresponding pure Fe_3O_4 nanoparticles [12,44]. The magnetic hysteresis loop indicates a

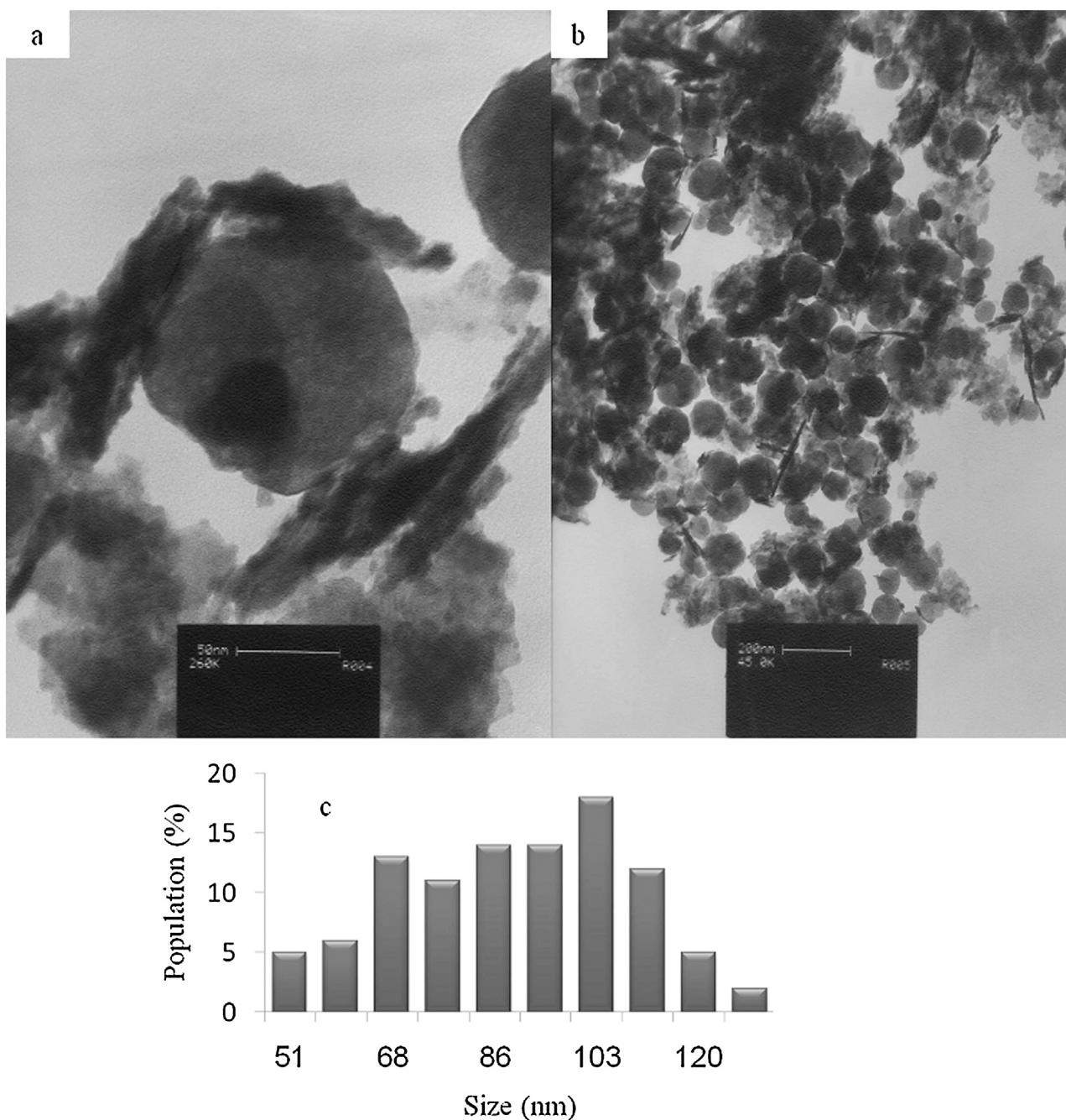


Fig. 1. TEM image of (a, b) as synthesized $\text{Fe}_3\text{O}_4/\text{Bi}_2\text{WO}_6$ nano-hybrid, and (c) particle size distribution of 3b (scale bar for (a): 50 nm and (b): 200 nm).

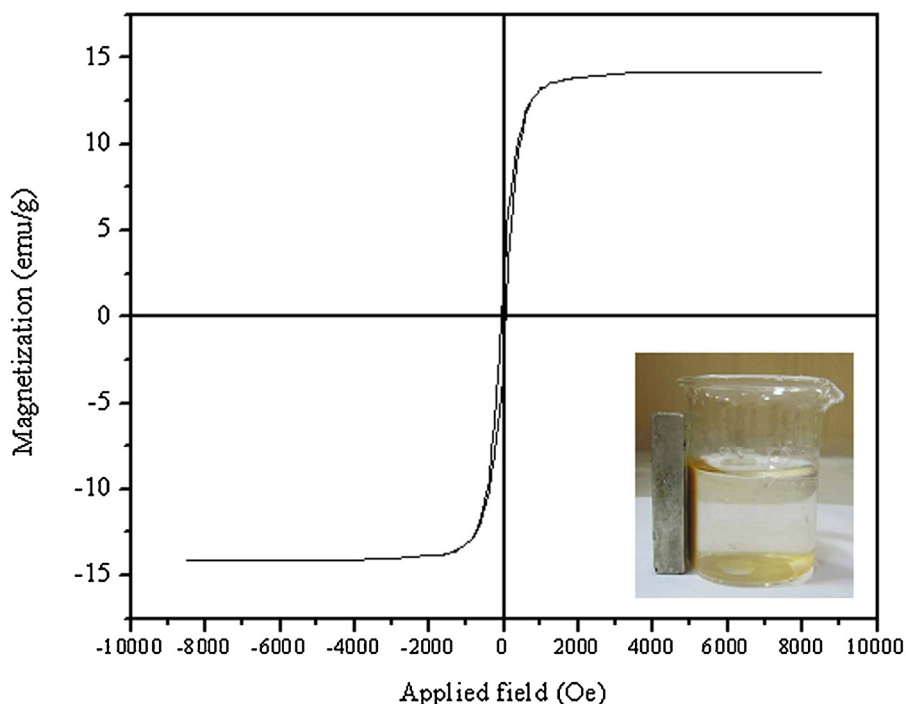


Fig. 2. Magnetization versus applied magnetic field for $\text{Fe}_3\text{O}_4/\text{Bi}_2\text{WO}_6$ nano hybrid.

small coercivity of about 80 Oe. The magnetic separability of $\text{Fe}_3\text{O}_4/\text{Bi}_2\text{WO}_6$ nano hybrids was examined in water by placing a magnet next to the glass beaker. The orange powders were absorbed by the magnet within a few seconds, thereby confirming that the products possessed good magnetic properties. This will allow convenient separation of magnetic- photocatalysis nano hybrids from the aqueous media with an external magnetic field.

XPS is a surface-sensitive technique that probes the outermost 5–10 nm of the sample [45]. The overall XPS spectra of the sample is shown in Fig. 3. The high-resolution XPS spectra of the primary elements in the nano hybrid is shown in Fig. 4. As can be seen, the

binding energy of $\text{Bi } 4f_{7/2}$, $\text{Bi } 4f_{5/2}$, $\text{W } 4f_{5/2}$, $\text{W } 4f_{7/2}$, and $\text{O } 1s$ were at 169.18, 174.33, 35.86, 38.86, and 540.33 eV, respectively [46]. The peaks at 711 and 721 eV were characteristic of Fe^{2+} and Fe^{3+} peaks [47]. However, the peak intensity of Fe (700–730 eV) is extremely weak due to thick Bi_2WO_6 shell.

The optical absorption properties of a semiconductor, which are relevant to the electronic structure, play a key role in determining its photocatalytic activity [48]. Fig. S3a. shows the absorption spectrum of $\text{Fe}_3\text{O}_4/\text{Bi}_2\text{WO}_6$ nano hybrids.

According to the results, the absorption edges of the sample are in the visible region (>400 nm). The band gaps of samples were

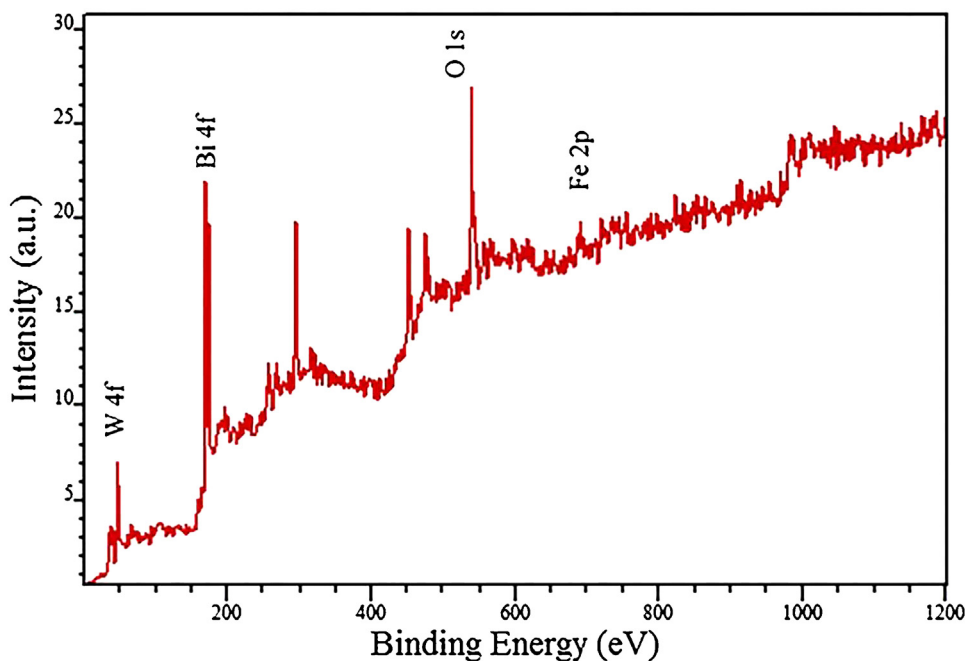


Fig. 3. XPS of $\text{Fe}_3\text{O}_4/\text{Bi}_2\text{WO}_6$ nano hybrid.

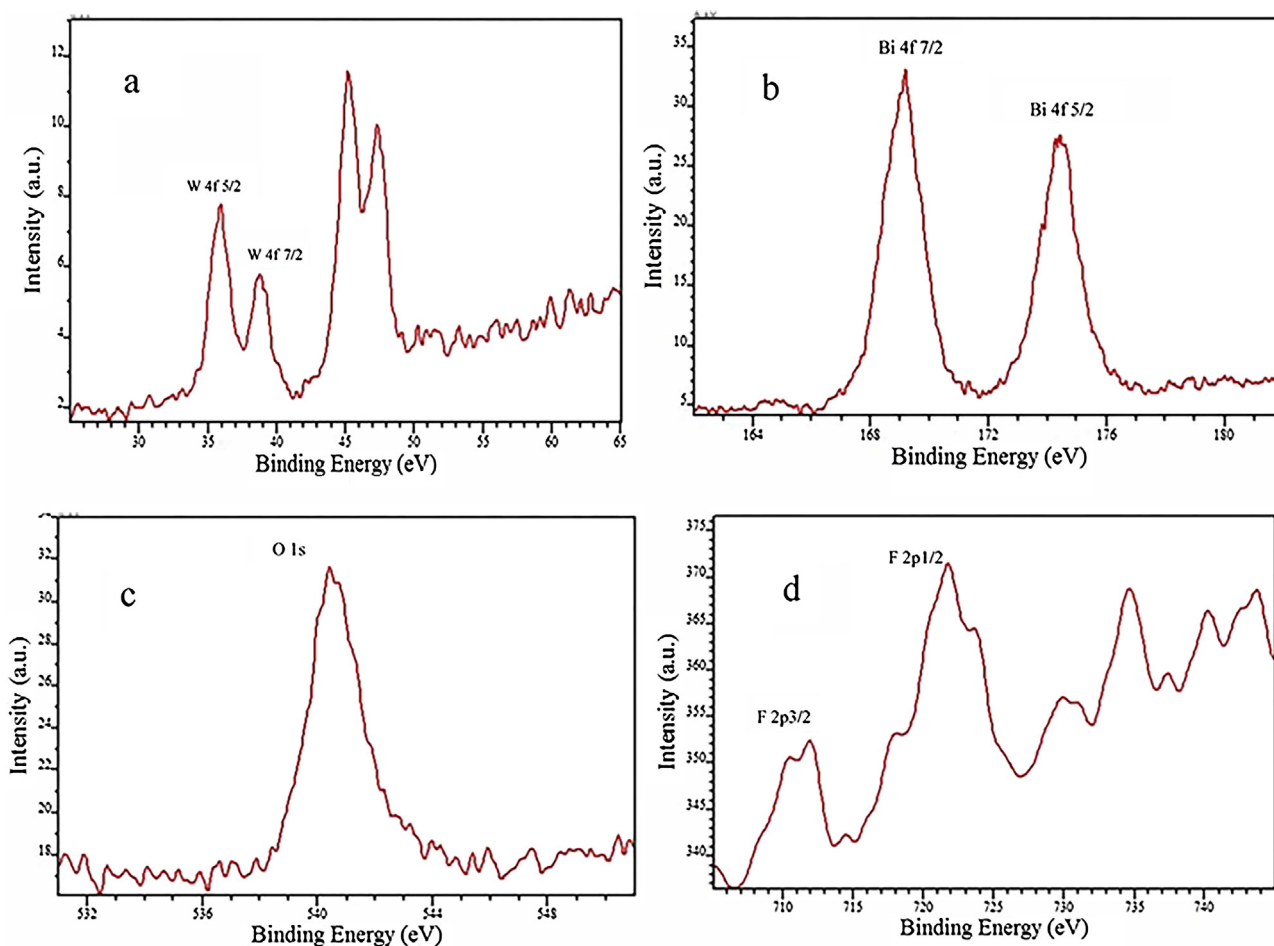


Fig. 4. XPS analysis of $\text{Fe}_3\text{O}_4/\text{Bi}_2\text{WO}_6$ nano hybrid: (a) W 4f; (b) Bi 4f; (c) O 1s; (d) Fe 2p.

calculated by the following formula [49]:

$$\alpha h\nu = A(h\nu - E_g)^n \quad (3)$$

where α , h , ν , E_g and A are absorption coefficient, Planck constant, light frequency, band gap energy, and measured absorbance respectively. In this formula, n is determined from the type of optical transition of semiconductor ($n = 1$ for direct transition and $n = 4$ for indirect transition) [49]. In the literature, a value of 1 has been reported for Bi_2WO_6 [50]. The direct band gap of $\text{Fe}_3\text{O}_4/\text{Bi}_2\text{WO}_6$ nano hybrids was determined based on the plot of $(\alpha h\nu)^{0.5}$ versus band gap energy ($h\nu$), and a value of 2.1 eV was obtained (Fig. S3b). The band gap values of Bi_2WO_6 reported in the literature are greater than that of $\text{Fe}_3\text{O}_4/\text{Bi}_2\text{WO}_6$ nano hybrids in this study [48,50]. Since the spectrum shape (Fig. 3Sa) is not steep, the visible light absorption can be due to transition from the impurity level [51].

The pH_{pzc} value of $\text{Fe}_3\text{O}_4/\text{Bi}_2\text{WO}_6$ nano hybrids is shown in Table S1. The pH_{pzc} is defined as the pH in which the net surface charge is zero. The surface charge is positive when the pH of solution is lower than pH_{pzc} , and vice versa. The pH_{pzc} of $\text{Fe}_3\text{O}_4/\text{Bi}_2\text{WO}_6$ nano hybrid was obtained about 6.2.

Photocatalytic degradation of IBP

The progress of the photocatalytic degradation of IBP under sunlight and dark conditions was followed by UV–vis spectroscopy using $\text{Fe}_3\text{O}_4/\text{Bi}_2\text{WO}_6$ nano hybrid. The main absorption band of IBP, which is located at 224 nm, is related to the benzene ring (see Fig. 3).

Effect of pH

In Fig. 5, the UV–vis spectrums of IBP degradation at different initial pHs of the solution under solar light irradiation and dark condition during 2 h are shown. According to Fig. 5a and b, the maximum degradation of IBP was obtained at pH 4.7. Given that the pK_a of the IBP is 4.9, the concentration of protonated and deprotonated forms of IBP at pH 4.7 are equal [7]. Under the dark condition (Fig. 5b), no significant degradation or removal of IBP in all pH ranges was observed except for the marginal adsorption at pH 4.7 (FTIR analysis confirmed this result). Thus, the degradation of IBP under sunlight is confirmed. The initial pH of the solution plays an important role in the photocatalytic degradation of organic pollutants. The surface charge of the catalyst can be changed depending on its point of zero charge (PZC) and chemical nature of the catalyst [11]. At pH values lower than pH_{pzc} , the surface of catalyst is protonated and therefore positively charged. On the contrary, at pH higher than pH_{pzc} , the surface is deprotonated and thus negatively charged [11,52]. The point of zero charge for $\text{Fe}_3\text{O}_4/\text{Bi}_2\text{WO}_6$ nano hybrid is close to 6.2. IBP is a weak acid with a pK_a of about 4.9, so lower pH will lead to the protonation of catalyst surface as well as the carboxyl group of IBP. The negative charge is increased at higher pH of the catalyst surface due to deprotonation of its surface and IBP. Under this condition, the predominance of electrostatic repulsion reduces the reaction rate. In acidic media, the surface of catalyst is protonated. According to the results, the acidic pH is suitable for the degradation of IBP under sunlight and adsorption onto the surface of photocatalyst under dark condition. Also, in the basic medium

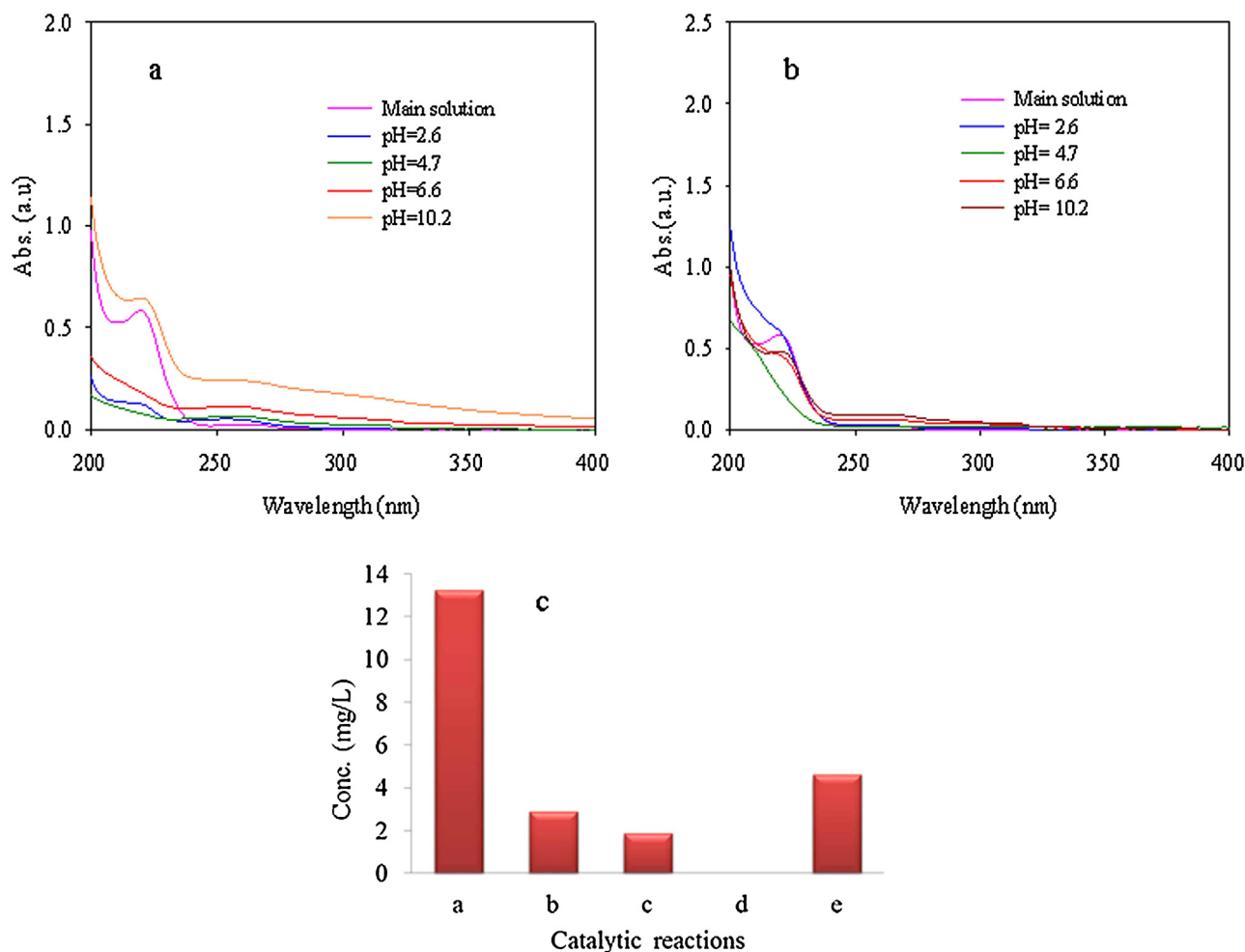


Fig. 5. UV-vis spectra of photocatalytic degradation of IBP on Fe₃O₄/Bi₂WO₆ at different pH after 2 h under (a) sunlight, (b) dark condition, and (c) the concentration of IBP as a function of pH by using Fe₃O₄/Bi₂WO₆ nano hybrids under sunlight (a) initial conc., (b) pH=2.6, (c) pH=4.7, (d) pH=4.7+40 μL H₂O₂, (e) pH=6.6, amount of photocatalyst=70 mg, initial conc.=10 mg L⁻¹, time=2 h).

(pH=10.0), the photo-degradation of IBP over Fe₃O₄/Bi₂WO₆ nano hybrids surface can be ignored. It seems that in low pH, the carboxylic group on the IBP molecule is shifted to the acidic form. Given the state of equilibrium, there are some carboxylic anions in the solution, which can be adsorbed on the surface. Also, the hydrogen bonding between protonated IBP and oxygen functional groups of catalyst surface could be happened. Furthermore, it is suggested that in high acidic pH (pH=2.6), the catalyst surface is more protonated than moderate acidic pH (pH=4.7) with greater positive charge on catalyst surface and IBP. Thus, the photo-degradation of IBP in moderate acidic pH was slightly higher than high acidic pH.

Given the application of POM (Keggin type) as an acidic agent in the synthesis of Fe₃O₄/Bi₂WO₆ nano hybrids, the higher degradation of IBP under solar light in acidic media might be due to the following reactions [48]:



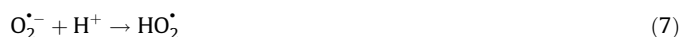
According to Eq. (3), the photo-excitation of POM in the structure of nano hybrid leads to (POM-S)*, which is followed by charge transfer and photo-reduction of POM:



The re-oxidation of POM upon exposure to O₂ is:



In acidic media, HO₂[•] is achieved in the following reaction:



As a result, the radical concentration is increased for the reaction with IBP.

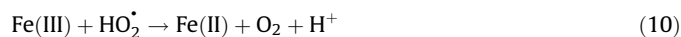
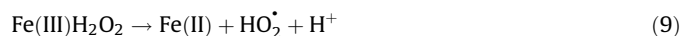
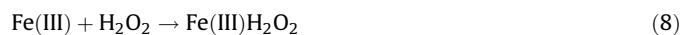
Hence, the higher degradation of IBP under solar irradiation and in acidic media might be due to following reasons:

- (1) Higher adsorption efficiency of IBP onto the surface of Fe₃O₄/Bi₂WO₆ nano hybrids, which makes the active site of catalysis more accessible to IBP molecules.
- (2) Role of POM in the degradation of IBP in the acidic media.

According to Fig. 5c, the photo-degradation of IBP over Fe₃O₄/Bi₂WO₆ nano hybrids depends on different pH values of the solution. The pH value of 4.7 in the aqueous solution increases the photocatalytic activity and completes the degradation of IBP by adding H₂O₂ (40 μL).

It is suggested that the hydrogen peroxide in contact with Fe(III) sites available on the surface of Fe₃O₄/Bi₂WO₆ photocatalyst can lead to the production of OH[•] radical as a chain reaction. Under acidic condition, the mechanism of H₂O₂ activation by Fe₃O₄/Bi₂WO₆ nano hybrids might resemble Eqs. (7)–(10) [53]. Firstly, Fe(III)-H₂O₂ complex is produced on the surface of photocatalyst (Eq. (7)). Then, the produced species is converted into Fe(II) and

HO_2^\bullet according to Eq. (8). Furthermore, Fe(II) species is generated on the surface of photocatalyst based on Eq. (9). All forms of Fe(II) species generated on the surface of photocatalyst could react with H_2O_2 and produce reactive radicals (HO_2^\bullet and HO^\bullet).



Effect of contact time

To evaluate the effect of contact time, the pH values were adjusted to 4.7. Fig. 6a and b shows the UV–vis spectra of IBP degradation at pH 4.7 under sunlight and dark conditions

respectively. As can be seen, no significant removal of IBP in the dark condition was observed. In the initial contact time, simultaneous side group oxidation and oxidation of the benzene ring of IBP were observed [48]. This was accompanied by the appearance of a new red-shift band at higher wavelengths (~ 252 nm) and broad band in the range of 240–300 nm. This observation confirms the production of intermediates and changed aromatic molecules at the beginning of photocatalytic reaction [11]. Fig. 6d shows the influence of contact time on the appearance of intermediates formed during the photocatalytic treatment of IBP based on UV–vis absorbance at ~ 252 nm. Intermediates appeared immediately after photocatalytic treatment of IBP and disappeared after 60 min. It is assumed that the degradation of IBP and intermediates was achieved after 60 min, which was due to high photocatalytic activity of $\text{Fe}_3\text{O}_4/\text{Bi}_2\text{WO}_6$ nanohybrid under solar light.

The higher activity of $\text{Fe}_3\text{O}_4/\text{Bi}_2\text{WO}_6$ nanohybrid can be attributed to more efficient separation of photo-induced electron–hole pairs in the composite due to the transfer of excited electrons of $\text{Fe}_3\text{O}_4/\text{Bi}_2\text{WO}_6$ to POM. Fig. 6c shows the effect of contact time on the photo-degradation of IBP over $\text{Fe}_3\text{O}_4/\text{Bi}_2\text{WO}_6$ photocatalyst under solar light.

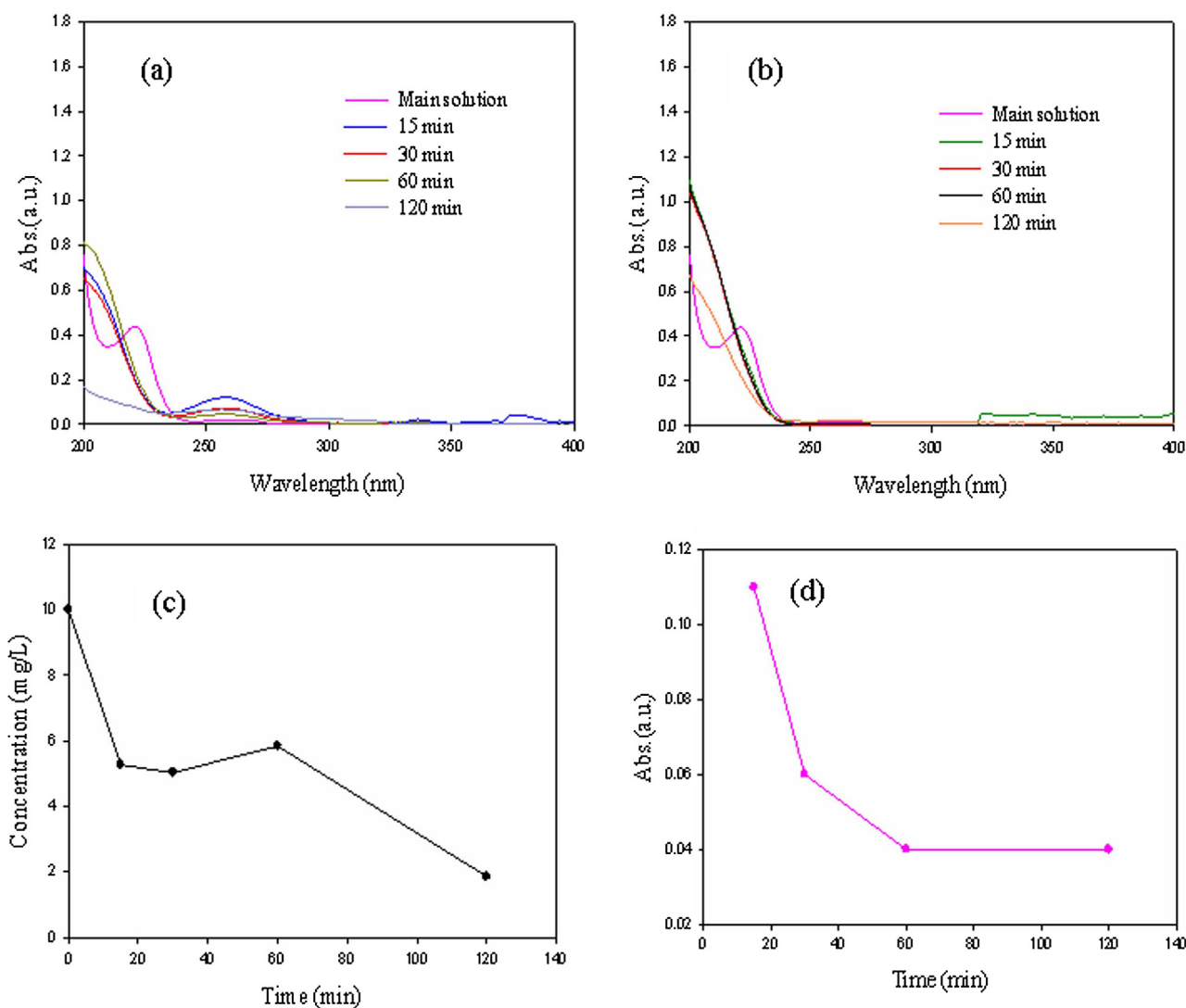


Fig. 6. UV–vis spectra of photocatalytic degradation of IBP on $\text{Fe}_3\text{O}_4/\text{Bi}_2\text{WO}_6$ at pH = 4.7 a) sunlight, b) dark condition, c) the concentration of IBP after photodegradation as a function of time by $\text{Fe}_3\text{O}_4/\text{Bi}_2\text{WO}_6$ nanohybrids under sunlight, and d) formation of intermediate products of IBP in aqueous solution under sunlight based on the change of UV–vis absorbance at $\lambda_{\text{max}} = 252$ nm (in the dark no intermediate was observed).

Stability and reusability of photocatalyst

From a practical point of view, the estimation of reusability and stability is of utmost importance. For this reason, the photo-degradation of IBP was repeated 5 times. The as-prepared $\text{Fe}_3\text{O}_4/\text{Bi}_2\text{WO}_6$ can be easily recycled by a simple magnetic filtration thanks to its good response to external magnetic field, thus avoiding the second pollution. As shown in the inset of Fig. 2, the magnetic photocatalyst could be conveniently collected from the solution by a magnet. After completing each run, $\text{Fe}_3\text{O}_4/\text{Bi}_2\text{WO}_6$ nano hybrids were separated from the solution by an external magnetic field. Then, the collected sample was repeatedly used in the next cycle. In each cycle, $\text{Fe}_3\text{O}_4/\text{Bi}_2\text{WO}_6$ nano hybrids (70 mg) were added to 50 mL of 10 mg L^{-1} IBP at pH=4.7 in 120 min. As shown in Fig. 7, IBP was decomposed in each cycle without any significant loss of activity after three cycles. It was also confirmed that the $\text{Fe}_3\text{O}_4/\text{Bi}_2\text{WO}_6$ nano hybrid was stable during photocatalytic oxidation of IBP for three cycles. Furthermore, there was no significant difference between FTIR spectrum of as-prepared $\text{Fe}_3\text{O}_4/\text{Bi}_2\text{WO}_6$ nano hybrids and the samples after degradation at pH=4.7 (Fig. S2).

Kinetics of photocatalytic degradation

To calculate the constant rate of photocatalytic degradation, Langmuir–Hinshelwood Model based on Eq. (12) was used [54].

$$r = \frac{dC}{dt} = \frac{k_r KC}{1 + KC} \quad (12)$$

In this equation, r ($\text{mg L}^{-1} \text{ min}^{-1}$), k_r ($\text{mg L}^{-1} \text{ min}^{-1}$), K (L mg^{-1}), C (mg L^{-1}) and t (min) are reaction rate, reaction rate constant, adsorption coefficient of the reactant, reactant concentration and illumination time, respectively. For extremely small C values, Eq. (13) can be converted into the following equation [54]:

$$r = \frac{dc}{dt} = k_r KC = kC \quad (13)$$

where k (min^{-1}) is the first-order rate constant.

If $t=0$ and $C=C_0$, Eq. (13) can be expressed as follows:

$$\ln \frac{C}{C_0} = -kt \quad (14)$$

where C_0 and C are initial concentrations of solution and IBP concentration after irradiation at various time intervals (t), respectively.

The photocatalytic degradation is apparent first-order kinetics based on the Langmuir–Hinshelwood model, and the rate

constants were determined by assuming pseudo first-order reaction kinetics [54].

The $\ln(C_0/C)$ plot shows a linear relationship with the irradiation time. The estimated rate constant is $k=0.0144 \text{ min}^{-1}$, with squares of linear correlation coefficients of $R^2=0.98$. The rate kinetic constant is dependent on the type of photoreactor with different parameters like geometries, dimensions, radiation sources, and flow conditions [34]. The incident photon flux is changed by altering reactor geometry [34]. It is suggested that the rate kinetic constant is not really constant and can be changed with different incident photon flux with different reactor geometry [34].

Approaching the mechanism

Studies show that the organic pollutant can be photo-degraded by photocatalytic oxidation (PCO) process. A PCO process includes a large number of main reactive species like h^+ , H_2O_2 , $\text{O}_2^{\cdot-}$, and $\text{OH}\cdot$ [48,55]. Thus, the effects of two scavengers were investigated to find the reaction mechanism. In this study, the isopropanol was added to the reaction system as $\text{OH}\cdot$ scavenger [56], and NaHCO_3 was introduced as $\text{OH}\cdot$ and a hole scavenger [55].

As shown in Fig. 8, the photodegradation of IBP was inhibited significantly in the presence of NaHCO_3 compared to absence of scavenger under the same conditions. Also, the addition of isopropanol to the IBP solution had weaker effects on the PCO progress of IBP compared to NaHCO_3 , indicating the main role of h^+ and the minor effect of $\text{OH}\cdot$ for IBP degradation.

In photocatalytic reactions, the activity of photocatalyst is affected by the recombination of photoinduced electrons and holes, which can reduce the quantum yield [57].

In this study, Bi_2WO_6 nanoparticles were coupled with some portions of the magnetite surface (Fig. 1b). Hence, it is possible that the excited electrons are transferred from the conducting band of nanophotocatalyst ($\text{Fe}_3\text{O}_4/\text{Bi}_2\text{WO}_6$) to the lower conducting band of Fe_3O_4 (Scheme 2) [24]. Furthermore, Scheme 2 shows the synergistic effect of POM and $\text{Fe}_3\text{O}_4/\text{Bi}_2\text{WO}_6$ nano hybrid.

It is assumed that the presence of POM in $\text{Fe}_3\text{O}_4/\text{Bi}_2\text{WO}_6$ photocatalyst improves photo-efficiency by retarding the fast recombination of a charge-pair (h^+e^-) on nano hybrids, and producing a strong oxidant $\text{O}_2^{\cdot-}$ [58]. As $\text{Fe}_3\text{O}_4/\text{Bi}_2\text{WO}_6$ is excited by the sunlight irradiation, the electron is transferred from its conducting band to the LUMO of the POM. Then, the adsorbed O_2 and H_2O_2 can easily trap an electron in the LUMO of the POM anion to yield the oxidizing species $\text{OH}\cdot$ followed by the attack of radicals to organic molecules. Therefore, the fast recombination of

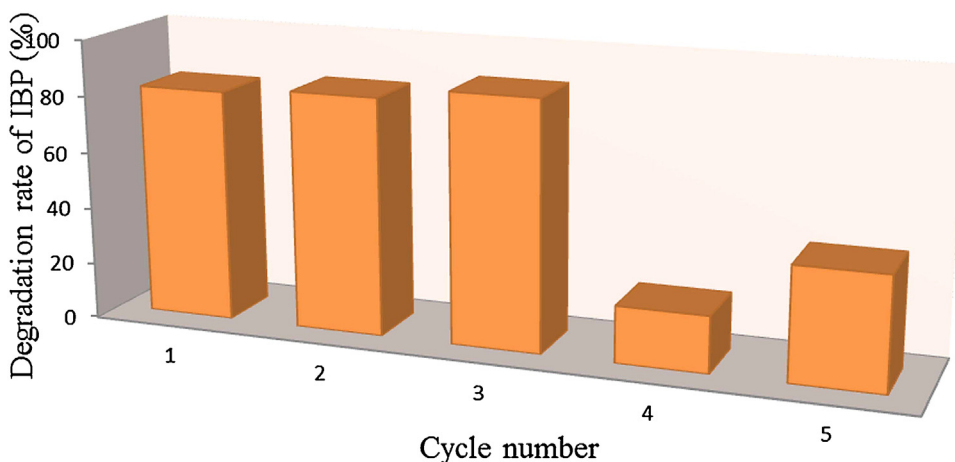


Fig. 7. The photo-degradation of IBP in five cycles on $\text{Fe}_3\text{O}_4/\text{Bi}_2\text{WO}_6$ nano hybrid.

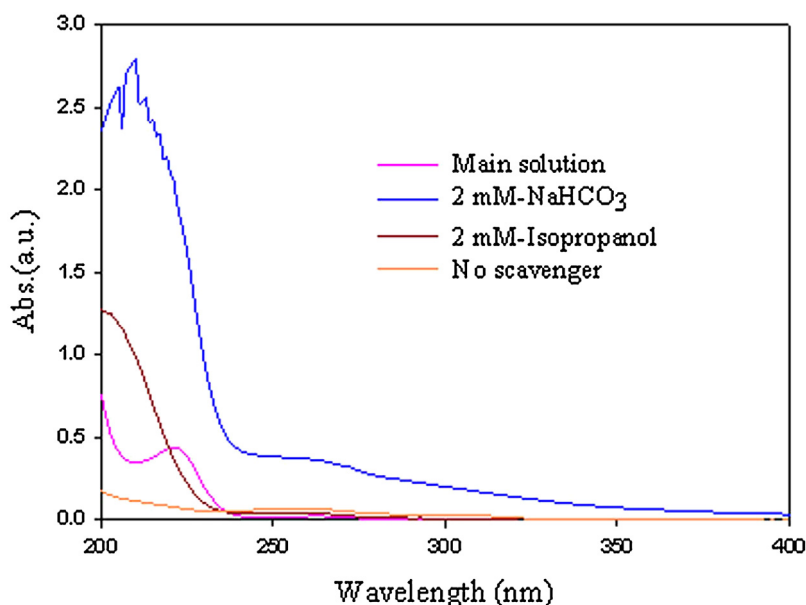
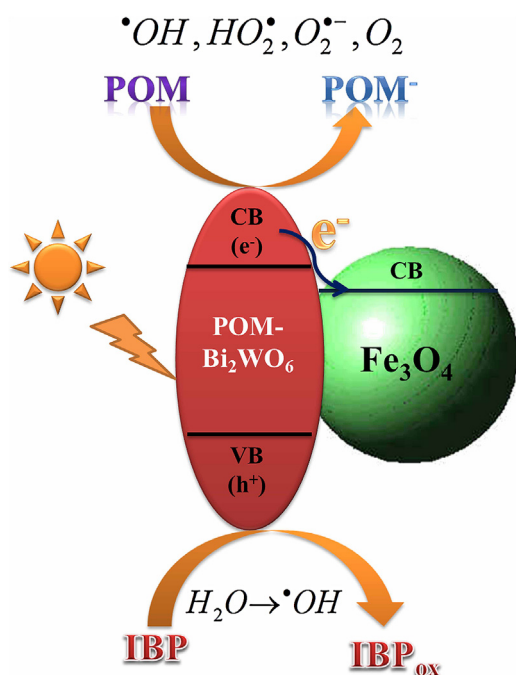


Fig. 8. Influence of different scavengers on the UV-vis spectra of IBP degradation onto $\text{Fe}_3\text{O}_4/\text{Bi}_2\text{WO}_6$ nano hybrids during 2 h at pH = 4.7 under sunlight.

photo-induced electron and holes can be retarded by the increased photocatalytic activity.

To detect intermediates after the photodegradation of IBP by $\text{Fe}_3\text{O}_4/\text{Bi}_2\text{WO}_6$ nano hybrids, the HPLC analysis was used. Fig. S5, shows the HPLC spectrums of the sample before and after photodegradation under solar light after 120 min (pH = 4.7, 40 μL H_2O_2). The results showed that the corresponding peak of IBP in t_r around 15 min disappeared after 120 min irradiation under solar light. In addition, no new peaks were observed after photodegradation under this condition, which confirmed thorough mineralization of IBP.



Scheme 2. Schematic diagram of the photocatalytic reaction of IBP on $\text{Fe}_3\text{O}_4/\text{Bi}_2\text{WO}_6$ nano hybrid.

Conclusion

In summary, $\text{Fe}_3\text{O}_4/\text{Bi}_2\text{WO}_6$ nano hybrids with photocatalytic activity were prepared in a two-step approach. Fe_3O_4 nanospheres were synthesized by the solvothermal method in polyol media and Bi_2WO_6 nanocrystals were formed in the subsequent hydrothermal process. In the preparation process of Bi_2WO_6 nanoparticles, tungstophosphoric acid hydrate ($\text{H}_3\text{PW}_{12}\text{O}_{40}$) was used as an acidic agent. Due to the synthesis of Fe_3O_4 nanoparticles in the ethylene glycol (EG), the surface of Fe_3O_4 nanosphere grew hydrophilic with the distribution of OH groups, which was favorable in terms of the connection of Bi_2WO_6 to the magnetite nanoparticles.

The test results of IBP decomposition indicated high photocatalytic activity of $\text{Fe}_3\text{O}_4/\text{Bi}_2\text{WO}_6$ nano hybrids under sunlight condition with the addition of hydrogen peroxide improving the efficiency of IBP degradation. Further, the removal of IBP in the dark condition could be ignored. According to the results, photogenerated holes (h^+) was found to be the main active species for degradation of IBP by $\text{Fe}_3\text{O}_4/\text{Bi}_2\text{WO}_6$ nano hybrids. The solar-Fenton degradation of IBP occurred on the surface of photocatalyst in the presence of H_2O_2 . Furthermore, the photocatalytic activity and magnetization properties of the magnetic-photocatalyst nano hybrids provide a promising solution for the degradation of water pollutants and photocatalyst recovery.

Acknowledgements

This work has been financially supported by the postdoc fellowship of Ferdowsi University of Mashhad and the Iranian National Science Foundation (INSF) (No. 92004798).

Appendix A. Supplementary data

Supplementary data associated with this article can be found, in the online version, at <http://dx.doi.org/10.1016/j.jiec.2017.03.008>.

References

- [1] J. Madhavan, F. Grieser, M. Ashokkumar, J. Hazard. Mater. 178 (1–3) (2010) 202.
- [2] B.G. Zheng, Z. Zheng, J.B. Zhang, X.Z. Luo, J.Q. Wang, Q. Liu, L.H. Wang, Desalination 276 (2011) 379.

- [3] H.R. Buser, T. Poiger, M.D. Müller, *Environ. Sci. Technol.* 33 (1999) 2529.
- [4] J.L. Santos, I. Aparicio, E. Alonso, Sevillecity (Spain) *Environ. Int.* 33 (2007) 596.
- [5] S. Esplugas, D. Bila, G. Krause, M. Dezotti, *J. Hazard. Mater.* 149 (2007) 631.
- [6] O. Gonzalez, C. Sans, S. Esplugas, *J. Hazard. Mater.* 146 (2007) 459.
- [7] E. Illés, E. Takács, A. Dombi, K. Gajda-Schranz, G. Rácz, K. Gonter, L. Wojnárovits, *Sci. Total Environ.* 447 (2013) 286.
- [8] F. Méndez-Arriagad, R.A. Torres-Palma, C. Pe'trier, S. Esplugas, J. Gimenez, C. Pulgarin, *Water Res.* 42 (2008) 4243.
- [9] F. Méndez-Arriag, S. Esplugas, J. Giménez, *Water Res.* 44 (2010) 589.
- [10] J. Madhavan, F. Grieser, M. Ashokkumar, *J. Hazard. Mater.* 178 (2010) 202.
- [11] J. Choina, H. Kosslicka, C. Fischer, G.-U. Flechsig, L. Frunzad, A. Schulz, *Appl. Catal. B* 129 (2013) 589.
- [12] S.-H. Chen, Z. Yin, S.-L. Luo, C.-T. Au, X.-J. Li, *Mater. Res. Bull.* 48 (2013) 725.
- [13] Y. Tang, Z. Jiang, G. Xing, A. Li, P.D. Kanhere, Y. Zhang, T. Sum, S. Li, X. Chen, Z. Dong, Z. Chen, *Adv. Funct. Mater.* 23 (2013) 2932.
- [14] Z. Jiang, Y. Tang, Q. Tay, Y. Zhang, O.I. Malys, D. Wang, J. Deng, Y. Lai, H. Zhou, X. Chen, Z. Dong, Z. Chen, *Adv. Energy Mater.* 3 (2013) 1368.
- [15] Y. Zhang, Y. Tang, X. Liu, Z. Dong, H.H. Hng, Z. Chen, T.C. Sum, X. Chen, *Small* 9 (2013) 996.
- [16] Y. Zhang, B. Wu, Y. Tang, D. Qi, N. Wang, X. Wang, X. Ma, T.C. Sum, X. Chen, *Small* 12 (2016) 2291.
- [17] C. Xu, X. Wei, Z. Ren, Y. Wang, G. Xu, G. Shen, G. Han, *Mater. Lett.* 63 (2009) 2194.
- [18] Y. Tsunoda, W. Sugimoto, Y. Sugahara, *Chem. Mater.* 15 (2003) 632.
- [19] Y.-L. Shi, W. Qiu, Y. Zheng, *J. Phys. Chem. Solids* 67 (2006) 2409.
- [20] R. Buonsanti, V. Grillo, E. Carlino, C. Giannini, F. Gozzo, Mar Garcia-Hernandez, M.A. Garcia, R. Cingolani, P.D. Cozzoli, *J. Am. Chem. Soc.* 132 (2010) 2437.
- [21] D. Beydoun, R. Amal, *Mater. Sci. Eng. B Solid* 94 (2002) 303.
- [22] L. Zhang, W. Wang, M. Shang, S. Sun, J. Xu, *J. Hazard. Mater.* 172 (2009) 1193.
- [23] Q. Gao, F. Chen, J. Zhang, G. Hong, J. Ni, X. Wei, D. Wang, *J. Magn. Magn. Mater.* 321 (2009) 1052.
- [24] L. Zhang, W. Wang, L. Zhou, M. Shang, S. Sun, *Appl. Catal B* 90 (2009) 458.
- [25] F.F. Bamoharram, A. Ahmadpour, M.M. Heravi, A. Ayati, H. Rashidi, B. Tanhaei, *Synth. React. Inorg. Met. Org. Nano-Met. Chem.* 42 (2012) 209.
- [26] A. Troupis, A. Hiskia, E. Papaconstantinou, *Angew. Chem. Int. Ed.* 41 (2002) 1911.
- [27] A. Ahmadpour, B. Tanhaei, F.F. Bamoharram, A. Ayati, M. Sillanpää, *Curr. Green, Nanoscience* 8 (2012) 880.
- [28] A. Ayati, A. Ahmadpour, F.F. Bamoharram, M.M. Heravi, H. Rashidi, B. Tanhaei, *Int. J. Nanosci. Nanotechnol.* 7 (2011) 87.
- [29] A. Ayati, A. Ahmadpour, F.F. Bamoharram, M.M. Heravi, M. Sillanpää, *Gold Bull.* 45 (2012) 145.
- [30] T. Rohani Bastami, M.H. Entezari, Q.H. Hu, S.B. Hartono, S.Z. Qiao, *Chem. Eng. J.* 210 (2012) 157.
- [31] T. Rohani Bastami, M.H. Entezari, C. Kwong, S. Qiao, *Front. Chem. Sci. Eng.* 8 (2014) 378.
- [32] I. Ali, Z.A. AL-Othman, A. Alwarthan, *J. Mol. Liq.* 219 (2016) 858.
- [33] J. Colina-Márquez, F. Machuca-Martínez, G. Li Puma, *Molecules* 20 (2017) 13354.
- [34] I. Grcic, G. Li Puma, *Environ. Sci. Technol.* 47 (2013) 13702.
- [35] G.A. Rance, D.H. Marsh, A.N. Khlobystov, *Chem. Phys. Lett.* 460 (2008) 230.
- [36] G. Li Puma, A. Brucato, *Catal. Today* 122 (2007) 78.
- [37] Z. Liu, F. Chen, Y. Gao, Y. Liu, P. Fang, S. Wang, *J. Mater. Chem. A* 1 (2013) 7027.
- [38] J. Yu, J. Xiong, B. Cheng, Y. Yu, J. Wang, *J. Solid State Chem.* 178 (2005) 968.
- [39] P. Tang, H. Chen, F. Cao, *Mater. Lett.* 68 (2012) 171.
- [40] S. Layek, A. Pandey, A. Pandey, H.C. Verma, *Int. J. Eng. Sci. Technol.* 2 (2010) 33.
- [41] Y. Guo, G. Zhang, H. Gan, *J. Synthesis, Colloid Interface Sci.* 369 (2012) 323.
- [42] M. Masteri-Farahani, J. Movassagh, F. Taghavi, P. Eghbali, F. Salimi, *J. Chem. Eng.* 184 (2012) 342.
- [43] M.-S. Gui, W.-D. Zhang, Y.-Q. Chang, Y.-X. Yu, *J. Chem. Eng.* 197 (2012) 283.
- [44] G.-Y. Zhang, Y. Feng, Q.-S. Wu, Y.-Y. Xu, D.-Z. Gao, *Mater. Res. Bull.* 47 (2012) 1919.
- [45] M. Wagner, *Anal. Chem.* 77 (2005) 911.
- [46] Y. Tian, L. Zhang, J. Zhang, *J. Alloys Compd.* 537 (2012) 24.
- [47] T. Rohani Bastami, M.H. Entezari, *Mater. Res. Bull.* 48 (2013) 3149.
- [48] L. Zhou, W. Wang, S. Liu, L. Zhang, H. Xu, W. Zhu, *J. Mol. Catal. A Chem.* 252 (2006) 120.
- [49] J. Wu, F. Duan, Y. Zheng, Y. Xie, *J. Phys. Chem. C* 111 (2007) 12866.
- [50] J. Cao, B. Luo, H. Lin, B. Xu, S. Chen, *J. Hazard. Mater.* 217–218 (2012) 107.
- [51] S. Guo, X. Li, F. H. g Wang, Z. Dong, J. Wu, *Colloid Interface Sci.* 369 (2012) 373.
- [52] T. Rohani Bastami, M.H. Entezari, *J. Chem. Eng.* 210 (2012) 510.
- [53] P.J. Vikesland, R.L. Valentine, *Environ. Sci. Technol.* 36 (2002) 512.
- [54] Y. He, N.B. Sutton, H.H.H. Rijnaarts, A.A.M. Langenhoff, *Appl. Catal. B* 182 (2016) 132.
- [55] X.F. Zhou, C. Hu, X.X. Hu, T.W. Peng, J.H. Qu, *J. Phys. Chem. C* 114 (2010) 2746.
- [56] W. Cui, H. Wang, Y. Liang, B. Han, L. Liu, J. Hu, *J. Chem. Eng.* 230 (2013) 10.
- [57] H.F. Cheng, B.B. Huang, Y. Dai, X.Y. Qin, X.Y. Zhang, *Langmuir* 26 (2010) 6618.
- [58] A. Dolbecq, P. Mialane, B. Keitab, L. Nadjo, *J. Mater. Chem.* 22 (2012) 24509.